An OTFT-driven rollable OLED display

Makoto Noda
Norihito Kobayashi
Mao Katsuhara
Akira Yumoto
Shinichi Ushikura
Ryouichi Yasuda
Nobukazu Hirai
Gen Yukawa
Iwao Yagi
Kazumasa Nomoto
Tetsuo Urabe

Abstract — An 80-µm-thick rollable AMOLED display driven by an OTFT is reported. The display was developed so as to be rollable in one direction with an integrated OTFT gate driver circuit. It was successfully operated by an originally developed organic semiconductor, a peri-xanthenoxanthene derivative. The display retained its initial electrical properties and picture quality even after being subjected to 1000 cycles of a roll-up-and-release test with a radius of 4 mm.

Keywords — *Organic TFT, rollable display, OLED display.*

DOI # 10.1889/JSID19.4.316

1 Introduction

Flexible active-matrix organic light-emitting-diode (AMOLED) displays have been receiving considerable attention because they are mechanically robust, lightweight, and thin, besides featuring excellent display properties. A rollable AMOLED display is attractive as a portable display device: The fact that it can be stored in a small space in a rolled-up condition greatly enhances its portability. Even though several types of flexible AMOLED displays have been developed over the past several years,[1–11] no rollable AMOLED displays have been reported to date. Organic TFT (OTFT) backplanes are a promising candidate for rollable displays because they are made of mechanically flexible organic materials. An OTFT has reportedly been successfully operated with a submillimeter bending radius.[12] Furthermore, OTFTs can be fabricated using solution processes, allowing a vacuum-free short-turn-around-time printing process. OLEDs are also suitable for rollable displays because they are all-solid-state display devices. Thus, OTFTs and OLEDs are conducive to being used in rollable displays. In this paper, we report on an OTFT-driven rollable OLED display.[13] An originally developed organic semiconductor, a *peri*-xanthnoxanthene (PXX) derivative,[14] was used for the active layer of the OTFT backplane, which improved the performance of OTFT, yielding mobility and subthreshold swing values of 0.4 cm^2/V-sec and 0.6 V/decade, respectively. An OTFT gate driver circuit was integrated into the backplane so that the display could be rolled up in one direction. The display showed no degradation in electrical properties or picture quality after 1000 roll-up-and-release cycles with a radius of 4 mm.

2 The rollable AMOLED display

Figures 1(a) and 1(b) show photographs of our newly developed OTFT-driven rollable AMOLED display operated in a flat and rolled-up condition, respectively. The display, with its thickness of only 80 µm, is so flexible that it can operate without failure in a rolled-up condition with a radius of 4 mm. Figure 2 shows the layout and circuit diagram of the display. In the 4.1-in. FWQVGA display, 240 × RGB signal

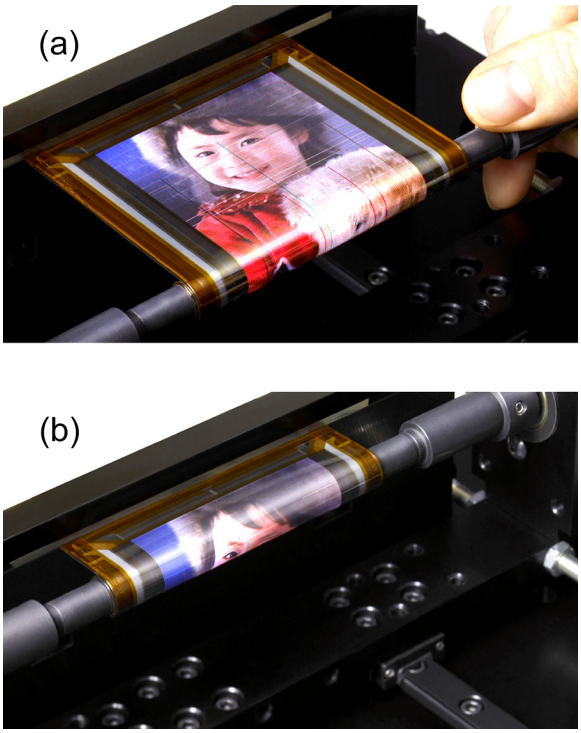

FIGURE 1 — Photographs of our rollable OTFT-driven OLED display (a) in a flat condition and (b) in a rolled-up condition with r = 4 mm.

The authors are with Sony Corp., Display Device Development Division, 4-16-1 Okata, Atsuki, Kanagawa 243-0021, Japan; telephone +81-46-226-2209, e-mail: MakotoA.Noda@jp.sony.com.

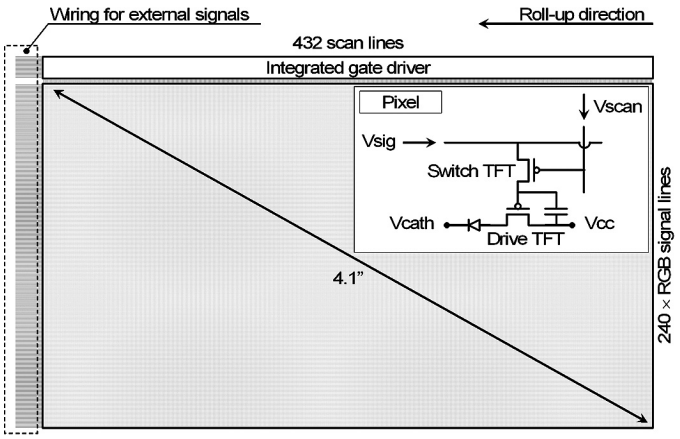

FIGURE 2 — Schematic design of the display. Inset shows schematic diagram of a pixel circuit.

lines are parallel to the roll-up direction, while 432 scanning lines are perpendicular to it. External source driver ICs for supplying signal voltages (V_{sig}) are employed. However, no external gate driver ICs are mounted on the display because an OTFT gate driver circuit supplying gate pulses (V_{scan}) is integrated on the side of the pixels, allowing the display to be rolled up. The inset of Fig. 2 shows a schematic diagram of the pixel circuit, which has a standard two-transistor one-capacitor architecture. The circuit parameters are designed so as to be operable at a frame rate of 60 Hz.

3 Flexible OTFT backplane

Figure 3 shows a schematic cross section of the display. We employed a stacked top-emission structure, which is advantageous to achieve a high resolution owing to the small footprint of a pixel in contrast to a side-by-side bottom-emission structure. The 20-μm-thick flexible substrate, on which OTFTs and OLEDs were integrated, and a 25-μm-thick cover film were employed. The resultant thickness of the display was 80 μm, which enhanced its flexibility.

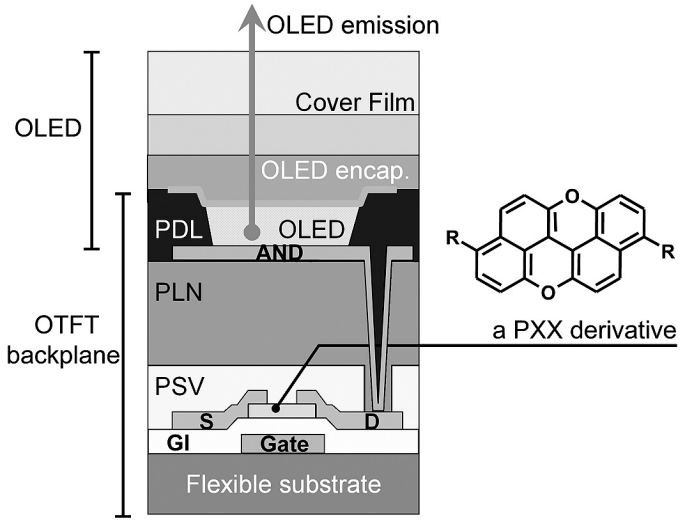

FIGURE 3 — Schematic cross section of the display.

The OTFT in the backplane had an inverted staggered-type structure with a channel length of 5 μm. First, the gate was formed by vacuum deposition and patterned by photolithography. Then, an originally developed gate insulator (GI) consisting of a blend of polyvinyl phenol with octadecyltrichloro-silan (PVP-OTS)[15] was formed by spin-coating. The gate insulator had a typical thickness of 400 nm and a relative dielectric constant of $\varepsilon = 4$. An originally developed organic semiconductor (OSC), a PXX derivative, was employed as an active layer. The PXX derivative is stable under ambient conditions and thermal stress because the reactive sites of the molecule are passivated by oxygen atoms, which suppresses the degradation of OTFT performance during the integration. After the deposition and patterning of the active layer and S/D metal electrodes, fluorinated polymer as passivation (PSV) and a conventional photopatternable resist as planarization layers (PLN) were formed by spin-coating. After the fabrication of through-holes, anode electrodes (AND) tied electrically to the drain of the drive OTFT were formed and the emission area was defined by the pixel-defining layer (PDL). As described above, a low-temperature solution process was employed for our OTFT backplane.[16] Figure 4 shows the integration flow of the OTFT backplane and the process temperature at each fabrication step. The maximum process temperature throughout the integration was 180°C. All the insulators consisted of mechanically soft polymers, allowing the display to be flexible and they were fabricated by a solution process.

Figure 5 shows the top view of a pixel in the OTFT backplane. A dense integration with a pixel pitch of 210 mm was achieved, which corresponds to a resolution of 121 ppi.

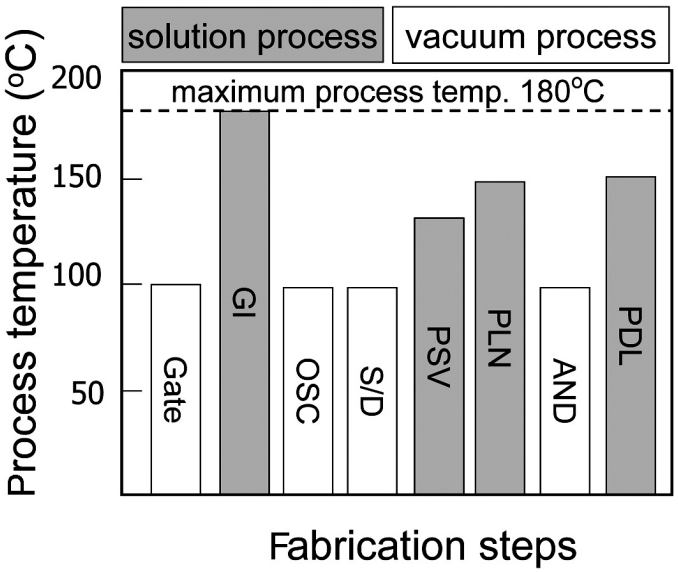

FIGURE 4 — Flow of integration processes and maximum process temperature at each fabrication step.

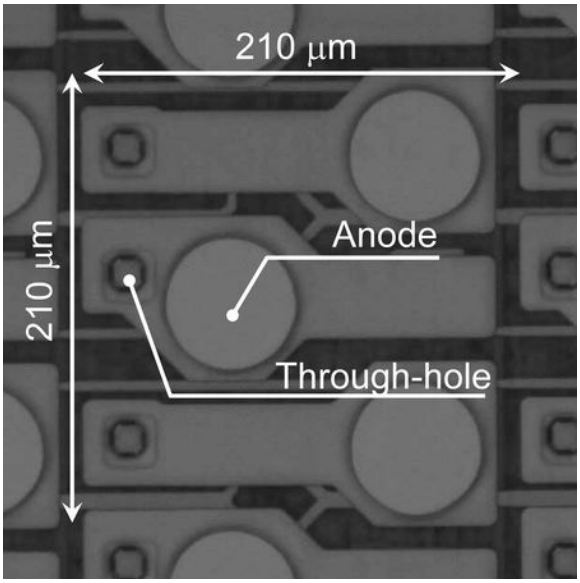

FIGURE 5 — Top view of a pixel.

4 Properties of rollable OLED display

Figure 6 shows a photograph of our 4.1-in. full-color OTFT-driven rollable OLED display, and Table 1 summarizes its specifications. The display was successfully driven by a PXX-TFT backplane. Not only still images, but also moving images at a frame rate of 60 Hz could be displayed.

TABLE 1 — Specifications of the display.

Display Size	4.1-in.Wide
Number of Pixels	432 × RGB × 240 (FWQVGA)
Pixel Size	210 μm × 210 μm
Resolution	121 ppi
Number of Colors	16,777,216
Peak Luminance	> 100 cd/m^2
Contrast Ratio	> 1000:1
Operation Scheme	2T-1C Voltage Programming
Scan Voltage	20 Vp-p
Signal Voltage	< 10 Vp-p
$V_{cc} - V_{cath}$	20 V
Thickness	80 μm
Bending Radius	4 mm

TABLE 2 — Comparison of electrical properties of pentacene TFT and PXX TFT.

Active layer	μ_{FE} (cm^2/V-sec)	S.S. (V/dec.)
pentacene	~0.1	1.2
PXX derivative	~0.4	0.6

FIGURE 6 — Photograph of 4.1-in. full-color rollable OTFT-driven FWQVGA OLED display.

5 Characterization of OTFT backplane

In this section, we discuss the properties of our newly developed PXX-TFT backplane with respect to its performance, driving voltage of the display, uniformity, and electrical sta-

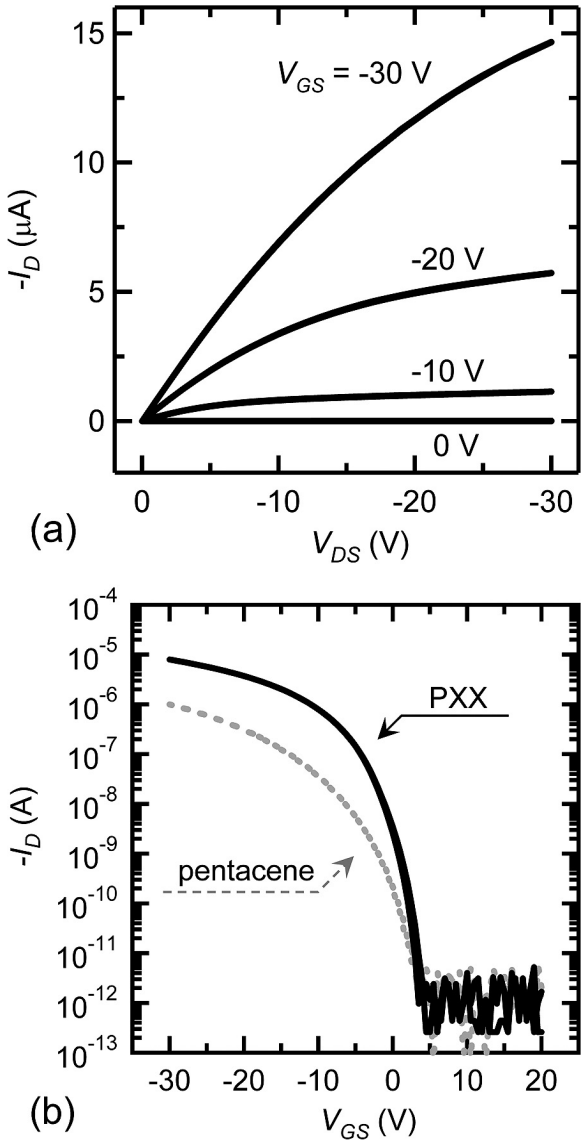

FIGURE 7 — (a) Output and (b) transfer characteristics of the drive TFT.

bility under DC bias stress. These characteristics of the PXX-TFT backplane are compared with our pentacene-TFT backplane. The PXX derivative led to improved performance, lower voltage driving of the display, and higher stability under DC bias-stress as compared to the pentacene-TFT backplane. The uniform on-current characteristics of the PXX TFT were comparable to those of the pentacene TFT.

5.1 Performance

Typical output and transfer characteristics of the drive TFT in the display are shown in Figs. 7(a) and 7(b). In the PXX TFT, the field-effect mobility (μ_{FE}) and subthreshold wing (*S.S.*) were 0.4 cm^2/V-sec and 0.6 V/decade, respectively. For a comparison of electrical characteristics, the transfer characteristics of a pentacene TFT in the backplane fabricated by the same process are also plotted in Fig. 7(b). Using the PXX derivative improved the performance of the OTFT not only in terms of the field-effect mobility, but also the subthreshold swing (see Table 2). This indicates that the current-contrast ratio of the PXX TFT is higher than that of the pentacene TFT at the same driving voltage. The driving voltage of the display with PXX-TFT backplane could be lower than that with pentacene-TFT backplane, as described in the next section.

5.2 Driving voltage of the display

Figure 8 shows gamma curves, *i.e.*, the relationship between display luminance and signal voltage, of the display with PXX-TFT backplane and, as a reference, of the pentacene-TFT-driven OLED display, which was demonstrated in our previous paper.[16] The display luminance from black to white level was well controlled by the signal voltage. The display could be driven at a signal voltage of 7 V to obtain a contrast ratio of 1000:1 with a peak luminance of 100 cd/m^2. The PXX-TFT backplane reduced the signal voltage by 30% with respect to the pentacene-TFT backplane for the same luminance and contrast ratio of display. This is due to the higher current-contrast ratio of the PXX-TFT backplane as compared to that of the pentacene-TFT backplane [see Fig. 7(b)]. Thus, the PXX-TFT backplane is effective in reducing power consumption.

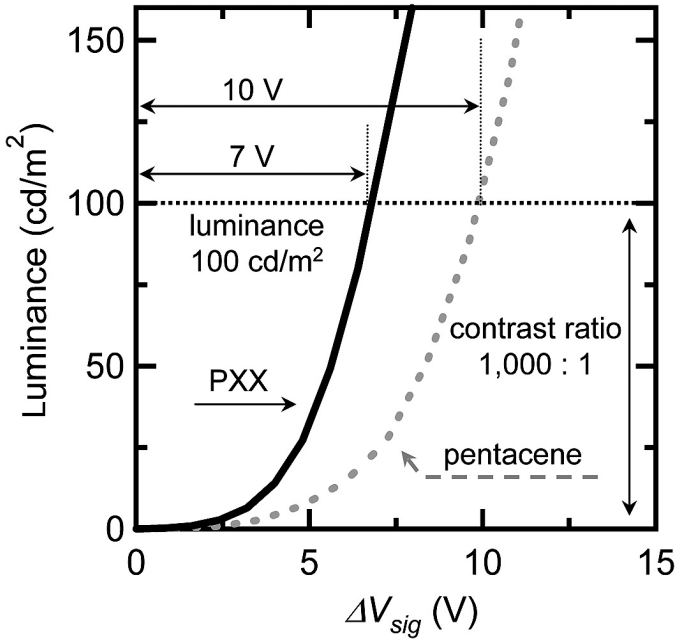

FIGURE 8 — Gamma curves of the display using PXX-TFT backplane (black) and pentacene-TFT backplane (gray).

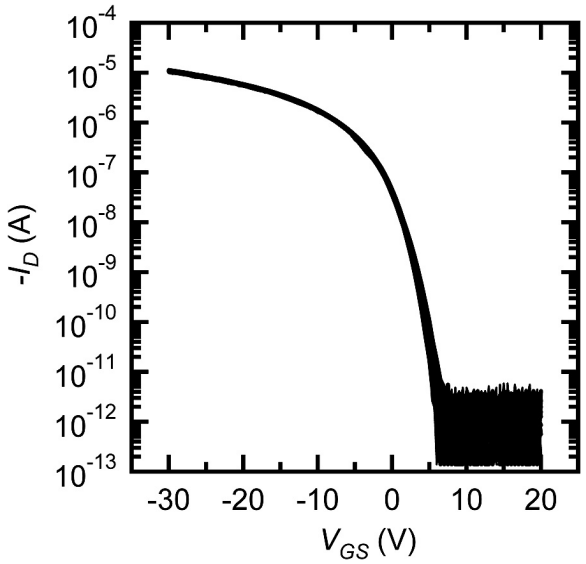

FIGURE 9 — Transfer characteristics of 47 PXX TFTs after integration of backplane.

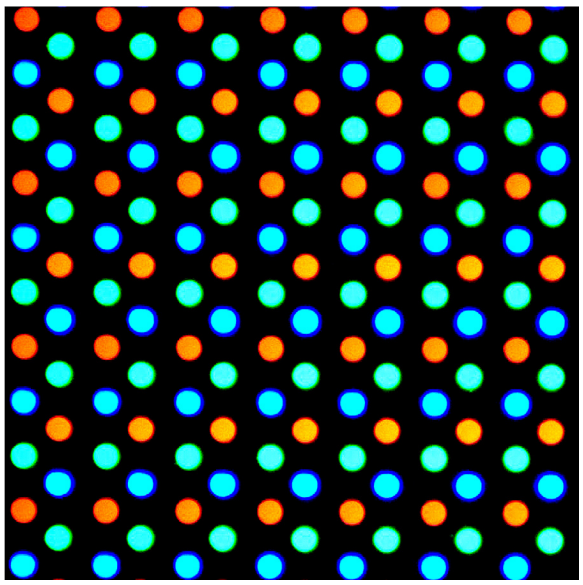

FIGURE 10 — Optical micrograph of emission from pixels in the display.

5.3 Uniformity

Figure 9 shows the transfer characteristics of 47 OTFTs with a channel length of 5 μm after integration of backplane. Uniform characteristics were achieved for the OTFTs, with a standard deviation of on-current of less than 5%, which is comparable to that of the pentacene TFT.[9]

Figure 10 shows an optical micrograph of emission from the pixels in the display. The luminance of each pixel was uniform over the short range, which is strongly supported by the uniform characteristics of the PXX TFT featuring the combination of a newly developed PXX derivative and an originally developed PVP-OTS gate insulator.

5.4 Bias-stress instability

A DC bias-stress test was performed on the PXX TFT after integration, under ambient conditions with an applied voltage of V_{GS} = –12 V and V_{DS} = –12 V.

Figure 11 shows transfer characteristics of the PXX TFT before and after applying the bias stress. There was no significant change in transfer characteristics upon applying a DC bias-stress for 1500 sec. Figure 12 shows the time dependence of V_{th} in PXX TFT and pentacene TFT as reference, fabricated using the same process. The variation in V_{th} in PXX TFT was negligibly small during the DC bias-stress test, while the DC bias-stress after 1500 sec caused a negative V_{th} shift of 0.1 V in pentacene TFT. These results indicate that the electrical stability of PXX TFT under bias stress is better than that of pentacene TFT, which is due to the improved interface between the active layer and gate insulator.

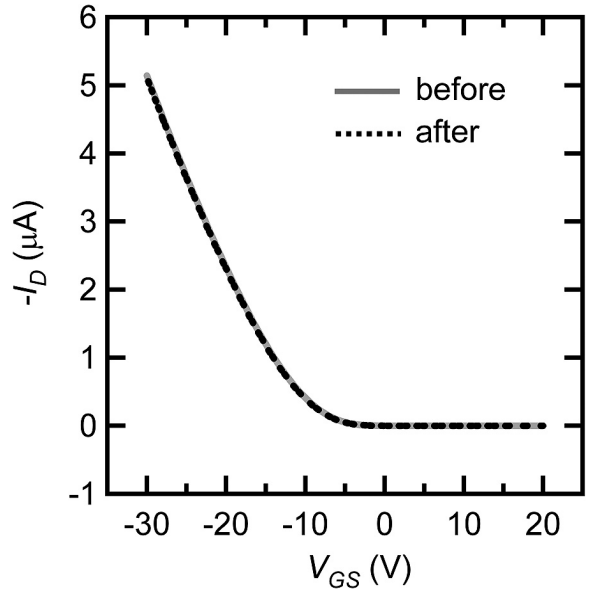

FIGURE 11 — Transfer characteristics of PXX TFT after integration of backplane, before (gray) and after (black) applying DC bias-stress for 1500 sec.

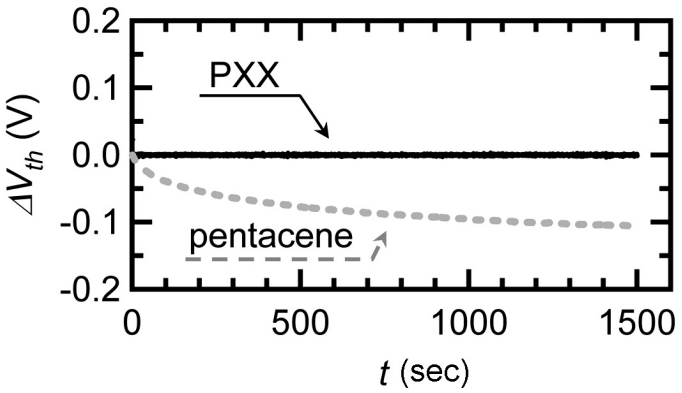

FIGURE 12 — Time dependence of V_{th} of PXX TFT (black) and pentacene TFT (gray) during DC bias-stress.

6 OTFT performance in bending state

It has been reported that the electrical characteristics of the flexible OTFT changed in a bending state. The change in electrical properties depended on the bending direction, bending radius, and device structure.[12,17] We have measured the mobility (μ) in the OTFT of our display while systematically varying the bending radius from 3 to 12 mm.

Figure 13 shows the dependence of the normalized mobility (μ/μ_0) on the bending radius of an OTFT in the display, where μ_0 is the mobility measured in a flat state. In the case of inward bending, the mobility increased with decreasing bending radius. By contrast, the mobility decreased with decreasing bending radius in outward bending. The change in mobility was less than 5% with a bending radius of 3 mm, under both inward and outward bending. This change was reversible (see Fig. 14). Measurement of

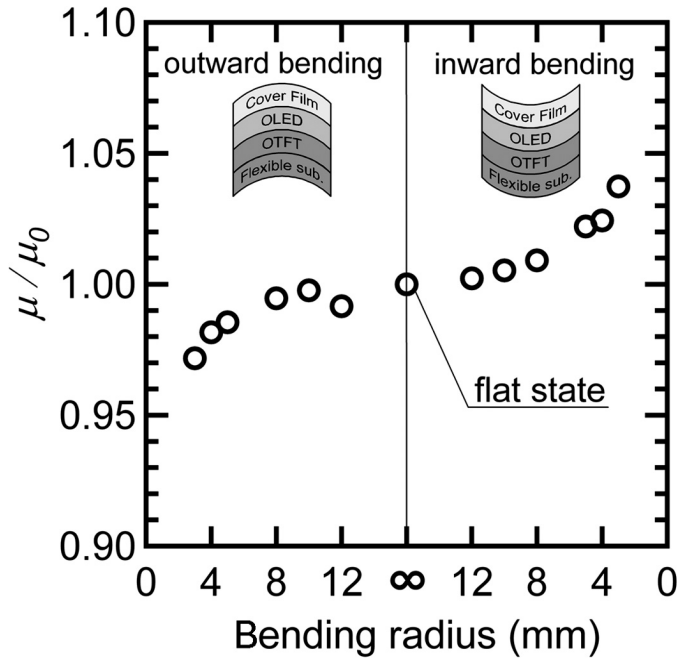

FIGURE 13 — Dependence of normalized mobility (μ/μ_0) on bending radius. Right and left figures correspond to inward and outward bending, respectively.

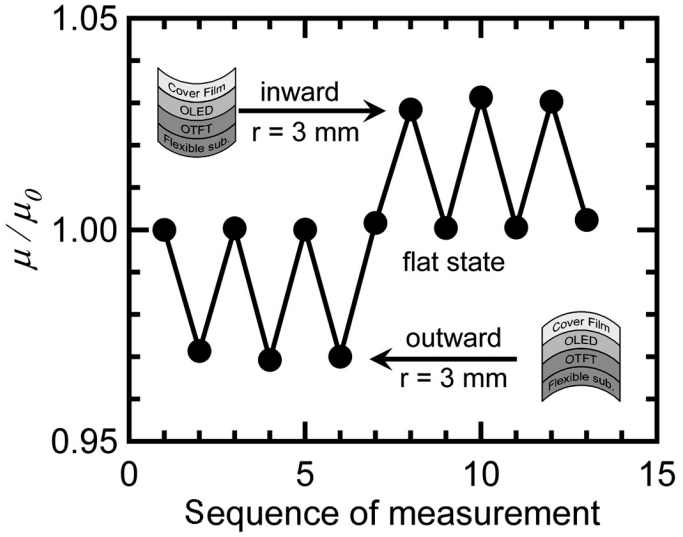

FIGURE 14 — Normalized mobility measured repeatedly under inward bending with r = 3 mm, outward bending with r = 3 mm, and flat state.

the mobility in a flat state was followed by measurement in a bending state with a radius of 3 mm. This series of measurements was repeated three times, both for outward and inward bending. The results indicate that the OTFT backplane can operate stably under both inward and outward bending with a radius of 3 mm.

7 Cyclic bending test

The mechanical stability of the OTFTs in the display is discussed. Figure 15(a) shows the schematic cross section of the device that was used for the cyclic bending tests, and Fig. 15(b) shows the cyclic bending test procedure. The device was bent outward along a cylinder with a radius of 4 mm. Then, it was returned to its flat state. The OTFT characteristics were measured in the flat state during the cyclic bending test.

Figure 16 shows the transfer characteristics of the OTFT in the display, measured before and after 100,000 cycles of bending with a radius of 4 mm. The OTFT showed no significant change in transfer characteristics after the cyclic bending test. Figure 17 shows both the on- and off-current as a function of the number of bending cycles. The

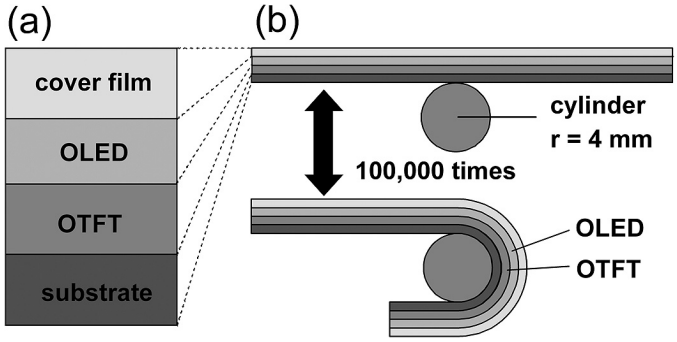

FIGURE 15 — (a) Schematic cross section of the device used for cyclic bending tests. (b) Procedure of cyclic bending test during which OTFT characteristics are measured in the flat state.

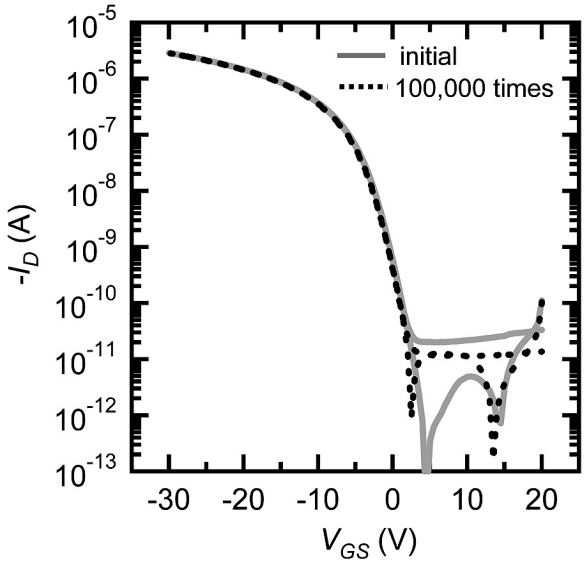

FIGURE 16 — Transfer characteristics of the pixel TFT measured before (gray) and after (black) 100,000 bending cycles with r = 4 mm.

change in the on-current was 1% even after 100,000 cycles. The off-current did not exhibit any obvious increase either. These results indicate that our OTFT backplane can drive a rollable OLED display stably under cyclic mechanical stress.

8 Roll-up-and-release test

We have also explored the mechanical stability of the display in a roll-up-and-release test, as shown in Figs. 1(a) and 1(b). First, the display was rolled up along a cylinder with a radius of 4 mm. Then, it was released completely. This roll-up-and-release cycle was repeated 1000 times. Figure 18 shows gamma curves of the display measured before and after the test. The display showed no significant degradation in

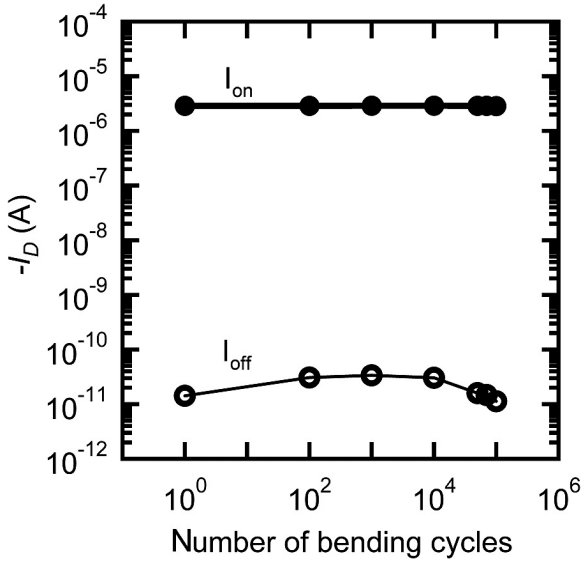

FIGURE 17 — On-current and off-current as a function of the number of bending cycles.

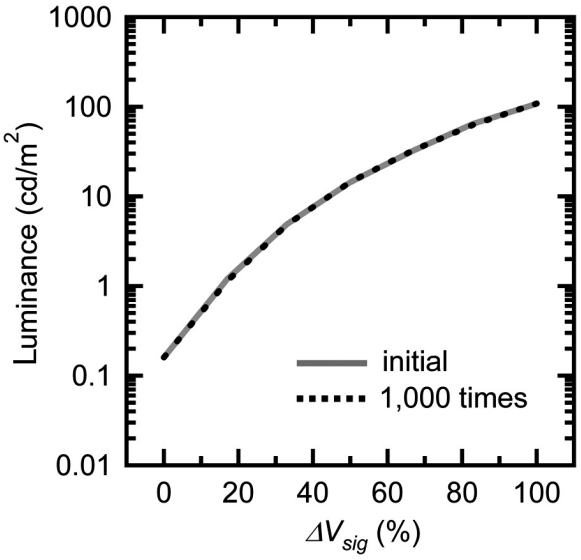

FIGURE 18 — Luminance characteristics of the display measured before (gray) and after (black) 1000 roll-up-and-release cycles with r = 4 mm.

gamma curves even after 1000 test cycles. This result indicates that neither the mobility of OTFT nor the efficiency of OLED changed during the test. The picture quality of the display after the test retained its initial state without additional defects, such as line defects, dark spots, or bright spots.

9 Conclusions

We have developed an OTFT-driven rollable OLED display with a thickness of 80 μm. The display was successfully operated by an OTFT with a newly developed organic semiconductor, a PXX derivative. By using this PXX derivative, the OTFT performance could be improved in terms of the field-effect mobility and subthreshold swing, as compared with a pentacene TFT. This led to lower voltage driving of the display and higher stability under DC bias-stress. The OTFT gate driver circuit was integrated into the backplane, which enabled the display to be rolled up. The display showed no degradation in electrical characteristics or picture quality after 1000 cycles of a 4-mm-radius roll-up-and-release test. The mechanical stability of our display is a direct function of the flexibility of the OTFT backplane consisting of mechanically soft organic materials. The present results indicate that our technology is promising for rollable displays.

Acknowledgments

The authors thank T. Sasaoka and T. Hirano for their kind suggestions in support of our project. The authors also thank N. Yoneya for technical advice regarding OTFT devices and T. Moriwaki for assistance with OLED fabrication.

References

1 S. H. Paek *et al.*, "Flexible display technology for a mass production using the improved etching technology," *SID Symposium Digest* **41**, 1047–1049 (2010).
2 R. Ma *et al.*, "Wearable 4-in. QVGA full-color-video flexible AMOLEDs for rugged applications," *J. Soc. Info. Display* **18**/1, 50–56 (2010).
3 S. An *et al.*, "2.8-inch WQVGA flexible AMOLED using high performance low temperature polysilicon TFT on plastic substrates," *SID Symposium Digest* **41**, 706–709 (2010).
4 J. Jang *et al.*, "TFT technologies for flexible displays," *SID Symposium Digest* **41**, 1143–1146 (2010).
5 J. H. Cheon *et al.*, "Active-matrix OLED on bendable metal foil," *IEEE Electron Dev.* **53**, 1273–1276 (2006).
6 D-U. Jin *et al.*, "Highly robust flexible AMOLED display on plastic substrate with new structure," *SID Symposium Digest* **41**, 703–705 (2010).
7 K. Arihara *et al.*, "Fabrication of flexible 4.7-inch QVGA AM-OLED panel driven by In-Ga-An-oxide TFTs with flexible color filter," *Proc. IDW '09*, 1613–1615 (2009).
8 H. Cheng *et al.*, "Plastic substrate and backplane for flexible AMOLED by sheet to sheet process," *Proc. IDW '09*, 1601–1603 (2009).
9 M. Katsuhara *et al.*, "A flexible OLED display with an OTFT backplane made by scalable manufacturing process," *J. Soc. Info. Display* **18**/6, 399–404 (2010).
10 M. Suzuki *et al.*, "5.8-inch phosphorescent color AM-OLED display driven by OTFTs on plastic substrate," *Proc. IDW '08*, 1515–1518 (2008).
11 I. Yagi *et al.*, "A full-color, top-emission AM-OLED display driven by OTFTs," *SID Symposium Digest* **38**, 1753–1756 (2007).
12 T. Sekitani *et al.*, "Submillimeter radius bendable organic field-effect transistors," *J. Non-Cryst. Solids* **352**, 1769–1773 (2006).
13 M. Noda *et al.*, "A rollable AM-OLED display driven by OTFTs," *SID Symposium Digest* **41**, 710–713 (2010).
14 N. Kobayashi *et al.*, "Stable peri-xanthenoxanthene thin-film transistors with efficient carrier injection," *Chem. Mater.* **21**, 552–556 (2009).
15 N. Yoneya *et al.*, "All-organic TFT-driven QQVGA active-matrix polymer-dispersed LCD with solution-processed insulator, electrodes, and wires," *SID Symposium Digest* **37**, 123–126 (2006).
16 N. Hirai *et al.*, "A flexible OTFT-OLED display using solution-processed organic dielectrics," *Proc. IMID '09*, 131–134 (2009).
17 T. Sekitani *et al.*, "Ultraflexible organic field-effect transistors embedded at a neutral strain Position," *Appl. Phys. Lett.* **87**, 173502(1)–(3) (2005).